IJAME

Int. J. of Applied Mechanics and Engineering, ????, vol.??, No.?, pp.????-????
DOI: 10.59441/ijame/226118

A COMPUTATIONAL INVESTIGATION ON THE IMPACTS OF CHEMICAL REACTIONS, JOULE HEATING ON MHD MAXWELL NANOFLUID FLOW PAST A POROUS VERTICAL STRETCHING SURFACE

Namala Yuvaraju[1,*], D. Hymavathi[2] and B. Shashidar Reddy[1]
[1]Department of Mathematics, Sreenidhi Institute of Science and Technology,
Hyderabad, Telangana, INDIA
[2]Department of Mathematics, University College of Science,
Mahatma Gandhi University, Nalgonda, Telangana, INDIA
E-mail: yuvaraju.n@sreenidhi.edu.in

The goal of this study is to determine how Joule heating, magnetic fields, and chemical reactions affect the flow of Maxwell nanofluid over a porous vertical stretching surface. This topic has several practical applications, such as cooling systems, polymer manufacture, and increased industrial efficiency. Heat treatment has several clinical applications, including improving drug delivery and treating cancer. Nanoparticles in the fluid achieve concentration by thermophoresis and move randomly via Brownian diffusion. The partial differential equations that govern flow and their accompanying boundary conditions can be transformed to non-dimensional form using appropriate similarity variables. The Runge-Kutta technique was used to solve transformed ordinary differential equations (ODEs). This shooting method converts the problem to an initial value problem (IVP), which the Runge-Kutta (RK) algorithm then utilizes to solve the boundary value problem. The results for numerous regulating flow factors are shown, and their implications on velocity, temperature, and concentration distributions are discussed. Drag factor, heat transfer coefficient, and mass transfer estimates are presented in a table format. The study's main findings show that increasing the Joule heating parameter improves concentration and temperature profiles while decreasing temperature distribution via an increase in the Prandtl value. The temperature profiles rise as the Lewis number, Brownian motion, and thermophoresis parameters increase. Concentration profiles decrease as the chemical reaction develops. There is remarkable agreement with previously published data.

Keywords: chemical reaction, Joule heating, Maxwell nanofluid, porous vertical stretching surface.

1. Introduction

The base fluids (water, kerosene, and ethylene glycol) are mixed with nanoparticles that range in size from 1 to $100\,nm$ to create nanofluids, a kind of engineering fluid. Here, we can choose base fluids according to certain uses, such as temperature and viscosity. Heat transfer systems, cooling electronics, medical devices, and thermal energy storage are just a few of the many uses for nanofluids. To better understand its rheology, numerous scholars have tried to elucidate the integrity of fluid dynamics in a range of real-world situations.

Maxwell nanofluid is a nanofluid characterized by viscosity qualities akin to those of Maxwell fluid. Nanofluids, comprising nanoparticles suspended in base fluids, improve thermal characteristics and have vital uses in a various sector. They increase heat transfer efficiency in vehicle heat exchangers, thermal management systems, and electronic cooling systems. Maxwell fluids' unique mix of viscous and elastic qualities makes them frequently employed in a various industry. Polymer processing, biological applications (such as blood flow analysis), and culinary preparation all make use of them. Mukhtar *et al.* [1] computed heat transfer in a flow of MNF subjected to magnetohydrodynamics (MHD) via a stretched flat surface, accounting for radiation. Srilatha *et al.* [2] investigated the impact of nanoparticle diameter on MNF flow and particle

* To whom correspondence should be addressed

deposition by thermophoresis. Anil Kumar and Dharmendar Reddy [3] investigated how heat and chemical interactions affect Maxwell fluid MHD BL flow on a stretchy surface containing nanoparticles. Ahmad *et al.* [4] investigated how slips and Joule heating affect MNF flow on a narrow surface. Irfan *et al.* [5] investigated heat sink/source and chemical reactions in the stagnation point flow of MNF. Sadiq *et al.* [6] described modeling and analysis of Maxwell nanofluids with mixed convection and the Darcy-Forchheimer connection. Himanshu *et al.* [7] investigated the impact of MHD Darcy-Forchheimer flow and double-diffusive Maxwell fluid modelling on a rotating stretchable surface using computer study. Lihong Zhang *et al.* [8] examines the 3D upper-convected Darcy-Forchheimer Maxwell (UCM) nanofluid flow over a stretching surface. Several MNF models have been used in recent studies [9-14].

For technical and engineering purposes, studying heat conduction in porous materials is essential. Permeability is the quality of a solid to allow heat to pass through it despite the presence of interconnected pores or empty spaces. Heat exchangers and cooling systems benefit from permeable media because they improve temperature dispersion. Oil and gas, insulating buildings, and energy storage systems are just a few of the many industries that rely on these porous materials. Enhancement of heat transport is an important and useful topic. Because of its significance, engineers and researchers are motivated to look for ways to advance their work and find solutions to enhance heat transmission. In addition to other techniques, the literature has examined the use of extended surfaces and fibres, nanofluids, external power sources in the form of electrohydrodynamics or magnetohydrodynamics, and porous media. One of the more successful approaches among the previously stated techniques is the use of magnetic fields, which has been investigated by Dulikravich and Lynn, Davidson, Sheikholeslami and Rokni [15-23]. M Sanjeeva Reddy *et al.* [24] discusses the effects of magnetic field chemical reactions and Soret-Dufour parameters on Maxwell nanofluid flow across a porous vertical stretching surface. Lots of different thermal applications are always looking for ways to optimize heat transmission, such as heat exchangers, electronic cooling, solar collectors, heat reservoirs, and cooling nuclear reactors. Heat transfer devices may function better if they were made of porous metals that have high solid thermal conductivities. H.J Xu *et al.* [25] discuss an overview of the principles and uses of heat conduction, convection, thermal radiation, and phase change heat transfer of nanofluids in porous medium. Bala Siddhulu *et al.* [32] studied the MHD viscous nanofluid due to convective stretching. Steady viscous dissipations and chemical reactions are examined in heat and mass transport. Mangamma *et al.* [33] investigated the effects of heat source, chemical reaction parameter and viscous dissipation on magnetohydrodynamic flow in the boundary layer of an incompressible fluid over a moving porous vertical plate. Mustafa [34] developed a generalized lubrication theory for the squeezing flow of a fluid film between non-linearly/exponentially extending or contracting barriers, unifying classical Stefan-Reynolds theory and contemporary soft-matter kinematics. The study investigated the dynamics of fluid flow and thermal transfer between two cylinders. The flow is generated exclusively by the expansion of the inner cylinder confined by the motionless outer cylinder, as described by Mustafa and Ioan Pop [35].

Unlike the Peltier effect, which only involves heat transfer between electrical connections, and Joule heating influences the whole electrical conductor. There are several devices and industrial uses for joule heating, which is also called resistive heating. The heating element is the part responsible for transforming electrical energy into heat, Joule heating, also known as resistive heating, is used in several technological and commercial operations. The portion that converts power to heat is referred to as the heating element. Electric heaters are frequently employed to warm structures when grid electricity is accessible. Electric stoves and ovens utilize Joule heating to cook food. With the use of heat from a soldering iron, conductive solder may be melted and used to join electrical components. Countless manufacturing operations rely on cartridge heaters. As a safety measure, electric fuses liquefy when exposed to currents above their melting threshold. Electronic cigarettes use Joule heating to vaporise liquid. Ehsan Ghaderi *et al.* [26] Analysed Joule heating's impact on heat transfer and entropy formation in MHD channel flow: a parametric investigation and ill-posed problem solution with PINNs. Yuvaraju *et al.* [27] describes the combined impact of Joule heating and velocity slip in MHD Casson-Williamson nanofluids passing through a stretching porous medium. Numerous writers such as [28, 29, 30] addressed research on nanofluids. Mixed convection combines the concepts of natural convection, which is induced by buoyancy forces owning to density differences, with forced convection, which is propelled by external sources such as fans or pumps. Applications of mixed convection heat transfer have garnered attention recently,

particularly in the fields of nuclear reactors, food processing, electronic cooling and lubrication technologies. G.A. Sheikhzadeh *et al.* [31] describes the combines variable thermal conductivity and variable viscosity to investigate the properties of mixed convection heat transfer in a lid-driven enclosure filled with nanofluids.

Prior research did not examine how Joule heating affects Maxwell fluids; instead, it focused on the maximum hydrodynamic drag (MHD) flow of nanofluids across permeable vertical stretching surface during Soret-Dufour, and chemical reactions effects. Without using Soret-Dufour parameters, this study attempts to examine Joule heating effects and the Maxwell nanofluid's MHD flow across the porous vertical stretching surface during chemical reaction. One way in which electricity may be used to create heat is via the phenomenon known as Joule heating. When nanoparticles are incorporated into the base fluid, two steps transpire: Brownian diffusion (random motion) and thermophoresis (concentration). Non-linear partial differential equations are transformed into non-linear ordinary differential equations by appropriate similarity transformations. This article describes a shooting approach for generating numerical results using the RK method. The findings for many regulating flow parameters are graphically shown, and their impacts on velocity, temperature, and concentration profiles are reviewed. There is a fair amount of consistency between the current study's results and those of other published studies. The physical interpretation of the problem's answers requires an understanding of the connection between mathematical results and actual events. The replies provide vital new information on how these factors interact and influence fluid behavior at a porous stretching surface.

2. Formulation of model

Think of a vertically stretchable surface with an incompressible 2-dimensional Maxwell nanofluid. The variables u and v stand for velocity's x and $y-$components correspondingly. Along the surface, the x-axis runs, and perpendicular to it, is the y-axis. A strong, perpendicular magnetic force, denoted as B_0, always acts on the sheet. Surface travels vertically with a linear velocity $u_w(x) = ax$, $a > 0$ which denotes stretching rate. Joule heating's cumulative effects are studied. We also considered variations in density and the impact of buoyancy. Until gravity is added to the mix, Boussinesq's computation does not take pressure fluctuations into account. Figure 1. depicts the physical interpretation of the idea.

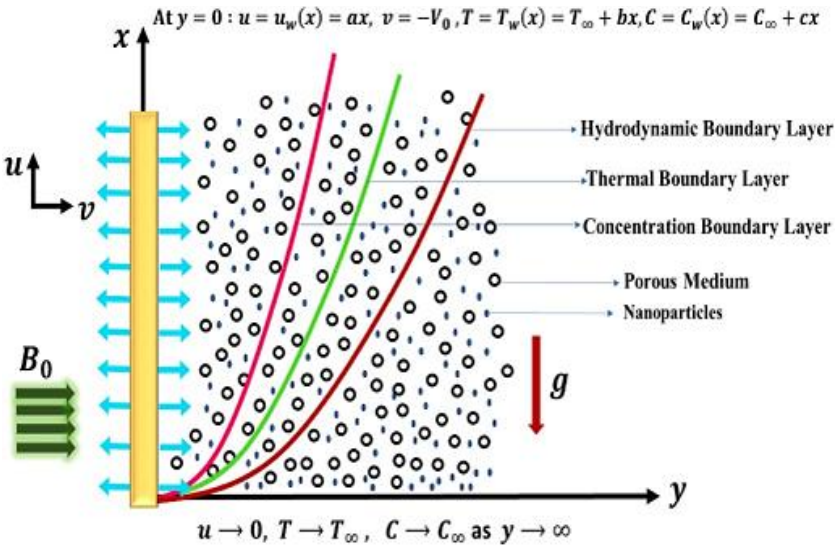


Fig.1. Physical interpretation.

$\tau = (\rho d)_p / (\rho d)_f$.

For a heated plate, $T_w > T_\infty \left(b > 0\right)$, whereas for cooling surface, $T_w < T_\infty \left(b > 0\right)$.
Governing equations [24] are:

$$\frac{\partial u}{\partial x}+\frac{\partial v}{\partial y}=0, \tag{2.1}$$

$$\begin{aligned} u\frac{\partial u}{\partial x}+v\frac{\partial u}{\partial y}=\nu\frac{\partial^2 u}{\partial y^2}-k_0\left(u^2\frac{\partial^2 u}{\partial x^2}+v^2\frac{\partial^2 u}{\partial y^2}+2uv\frac{\partial^2 u}{\partial x\partial y}\right)+ \\ -\frac{\sigma B_0^2}{\rho}u-\frac{\nu}{k}u+g\left[\beta_T\left(T-T_\infty\right)+\beta_C\left(C-C_\infty\right)\right] \end{aligned}, \tag{2.2}$$

$$u\frac{\partial T}{\partial x}+v\frac{\partial T}{\partial y}=\alpha\frac{\partial^2 T}{\partial y^2}+\tau\left[D_B\frac{\partial C}{\partial y}\frac{\partial T}{\partial y}+\frac{D_T}{T_\infty}\left(\frac{\partial T}{\partial y}\right)^2\right]+\frac{\sigma B_0^2}{\rho C_p}u^2, \tag{2.3}$$

$$u\frac{\partial C}{\partial x}+v\frac{\partial C}{\partial y}=D_B\frac{\partial^2 C}{\partial y^2}+\frac{D_T}{T_\infty}\frac{\partial^2 T}{\partial y^2}-kr\left(C-C_\infty\right). \tag{2.4}$$

With appropriate boundary conditions:

$$\begin{aligned} &u=u_w\left(x\right)=ax,\quad v=-V_0,\quad T=T_w\left(x\right)=T_\infty+bx,\quad C=C_w\left(x\right)=C_\infty+cx:y=0, \\ &u=0,\quad T=T_\infty,\quad C=C_\infty:y\to\infty. \end{aligned} \tag{2.5}$$

Here are the relations that have been introduced:

$$u=\frac{\partial\psi}{\partial y},\quad v=-\frac{\partial\psi}{\partial x},\quad \psi=x\sqrt{a\nu}f\left(\eta\right),\quad \eta=\sqrt{\frac{a}{\nu}}y,\quad \theta=\frac{T-T_\infty}{T_w-T_\infty},\quad \phi=\frac{C-C_\infty}{C_w-C_\infty}, \tag{2.6}$$

where ψ is the flow's stream function.
If we plug Eq.(2.6) into Eqs (2.2)-(2.4), we get these non-linear ODEqs:

$$f'''+ff''-\left(f'\right)^2+B\left(2fff''-f^2f'''\right)-Pf'-Mf'+\lambda_1\theta+\lambda_2\phi=0, \tag{2.7}$$

$$\theta''+Prf\theta'++PrNt\left(\theta'\right)^2+PrNb\theta'\phi'+PrJ\left(f'\right)^2=0, \tag{2.8}$$

$$Nb\phi''+Nt\theta''+NbPrLef\phi'-NbPrLeA\phi=0. \tag{2.9}$$

The altered boundary conditions Eq.(2.5) are:

$$\begin{aligned} &f\left(0\right)=S,\quad f'\left(0\right)=1,\quad \theta\left(0\right)=1,\quad \phi\left(0\right)=1, \\ &f'\left(\infty\right)=0,\quad \theta\left(\infty\right)=0,\quad \phi\left(\infty\right)=0, \end{aligned} \tag{2.10}$$

$$Pr=\frac{\nu}{\alpha},\quad Le=\frac{\alpha}{D_B},\quad B=ak_0,\quad M=\frac{\sigma B_0^2}{\rho a},\quad Nt=\frac{\tau D_T\left(T_w-T_\infty\right)}{T_\infty\nu},\quad Nb=\frac{\tau D_B\left(C_w-C_\infty\right)}{\nu},$$

where:

$$J=\frac{\sigma B_0^2 ax^2}{\rho C_p\left(T_w-T_\infty\right)},\quad Sc=\frac{\nu}{D_B},\quad P=\frac{\nu}{ka},\quad A=\frac{Kr}{a},\quad \lambda_1=\frac{g\beta_T\left(T_w-T_\infty\right)}{a^2x},\quad \lambda_2=\frac{g\beta_c\left(C_w-C_\infty\right)}{a^2x}.$$

What follows is a definition of the relevant physical quantities such as skin friction, Nusselt number and Sherwood number.

$$C_f=\frac{\tau_w}{\rho u_w^2},\ Nu_x=\frac{xq_w}{k\left(T_w-T_\infty\right)},\ Sh_x=\frac{xq_m}{D_B\left(C_w-C_\infty\right)},\tag{2.11}$$

$$q_m=-D_B\left(\frac{\partial C}{\partial y}\right)_{y=0}\quad \text{is mass flux},\quad q_w=-k\left(\frac{\partial T}{\partial y}\right)_{y=0}\quad \text{is heat flux},$$

where: (2.12)

$$\tau_w=\mu\left(1+B\right)\left(\frac{\partial T}{\partial y}\right)_{y=0}\quad \text{is drag factor along the sheet.}$$

What follows is a dimensionless representation of the quantities given in Eq.(2.12):

$$Re_x^{\frac{1}{2}}C_f=\left(1+B\right)f''(0),\ \frac{Nu_x}{Re_x^{\frac{1}{2}}}=\theta'(0),\ \frac{Sh_x}{Re_x^{\frac{1}{2}}}=-\phi'(0),\tag{2.13}$$

where: $Re_x=\frac{xu_w}{\nu}$ is the local Reynolds number.

3. Method of solution

Following the most effective numerical strategy based on the R-K method technique, we solved ODEs Eq. (2.7) through Eq. (2.9) together with their corresponding initial and boundary conditions. The symbolic programming MATLAB is used to generate the numerical solutions. Let:

$$f=y_1,\quad f'=y_1'=y_2,\quad f''=y_2'=y_3,\quad f'''=y_3',$$

$$\theta=y_4,\quad \theta'=y_4'=y_5,\quad \theta''=y_5',$$

$$\phi=y_6,\quad \phi'=y_6'=y_7,\quad \phi''=y_7',$$

$$\Rightarrow y_1'=y_2,\quad y_1(0)=S=\frac{V_0}{\sqrt{a\nu}},\quad y_2(0)=1,\quad y_4(0)=1,\quad y_6(0)=1.$$

After taking into account the characteristics listed above, we came to the following conclusions:

$$f''' = y_3' = \frac{1}{1 - By_1^2}\left[(y_2)^2 - y_1 y_3 - 2By_1 y_2 y_3 + My_2 + Py_2 - \lambda_1 y_4 - \lambda_2 y_6 \right], \tag{3.1}$$

$$\theta'' = y_5' = -Pry_1 y_5 - PrNt(y_5)^2 - PrNby_5 y_7 - PrJ(y_2)^2, \tag{3.2}$$

$$\phi'' = y_7' = \frac{1}{Nb}\left[NbPrLeAy_6 - Nty_5' - NbPrLey_1 y_5 \right] = \frac{1}{Nb}\left[NbPrLeAy_6 + Nt\left\{ Pry_1 y_5 + PrNt(y_5)^2 + PrNby_5 y_7 + PrJ(y_2)^2 \right\} - NbPrLey_1 y_5 \right]. \tag{3.3}$$

You may use fourth-order R-K method to integrate the seven first-order simultaneous equations and their conditions that were described before. The technique is reiterated until the results achieve the expected accuracy of 10^{-7} to fulfill convergence requirement.

3.1. Flow chart of the Runge-Kutta method

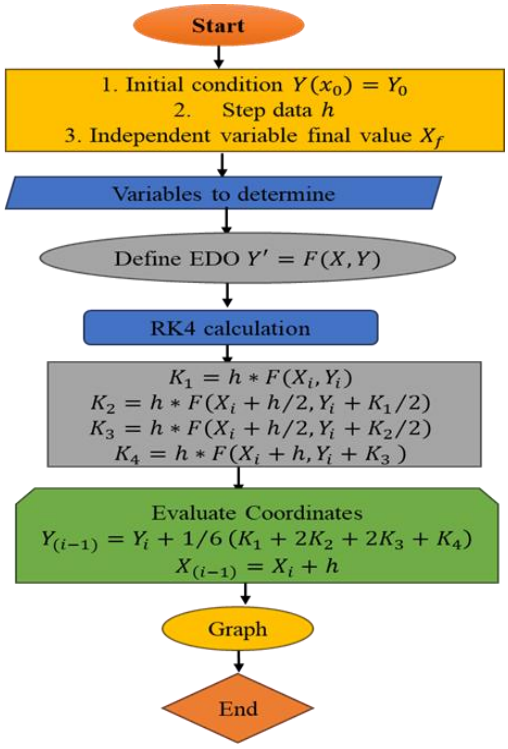


Fig.2. Flow chart of the Runge-Kutta method.

4. Results and discussion

This study details the effects of Joule heating and chemical reactions caused by magnetic fields on the flow of Maxwell nanofluid over a vertically extended porous surface.

When it comes to solving ODEs in regular domains, the conventional (R-K) method is a reliable strategy. Because it is inexpensive, easy to code, and accurate to five decimal places, it is one of the most popular methods.

The impact of a few nondimensional parameters on velocity, temperature, and concentration distribution is shown in Figs 3-13. There is a significant agreement between the case study results and previous research [24].

Figure 3 depicts the impact of Prandtl number Pr on the thermal field. A variety of realistic Prandtl numbers are represented in the temperature circulation. When studying the distribution of temperatures and the properties of heat transport across a stretched or contracted sheet, the Prandtl number plays a crucial role. The graph shows that the temperature dropped as Pr estimations rose. This phenomenon is explained by the fact that a fluid with higher Prandtl number has reduced thermal conductivity. Thermal boundary layer is thinner and conduction is limited as the temperature drops due to decreased thermal conductivity. A relative mass of momentum and thermal black bodies is determined in heat transfer problems by Prandtl number and heat sink value.

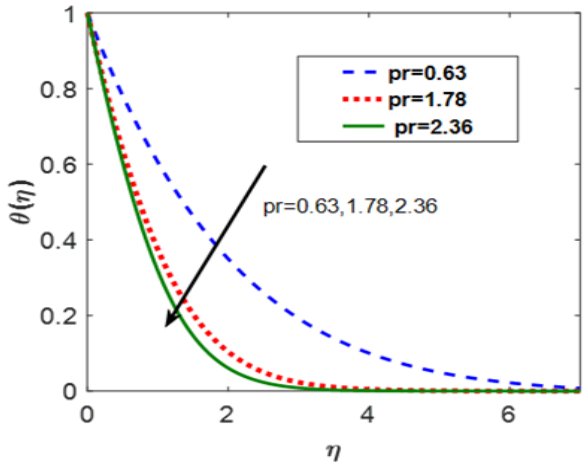


Fig.3. Temperature v/s Prandtl number.

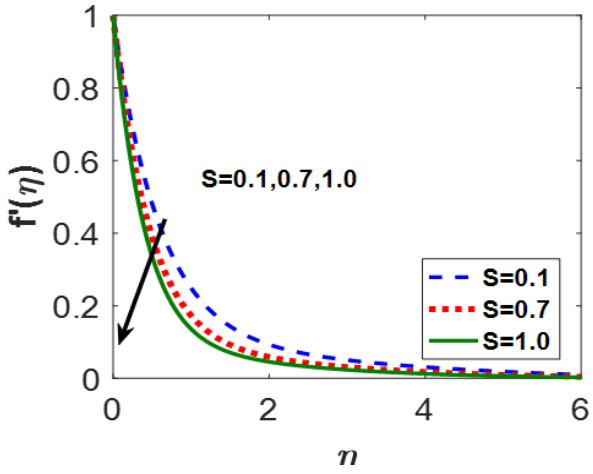


Fig.4. Velocity v/s suction parameter.

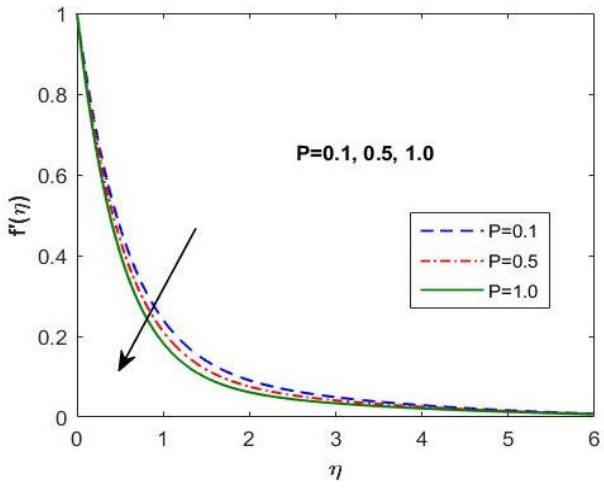


Fig.5. Velocity v/s porosity parameter.

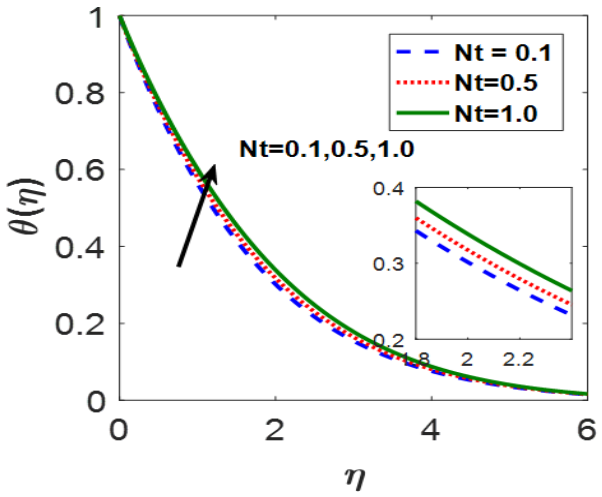


Fig.6. Temperature v/s thermophoresis.

The operation of suction is shown in Fig.4. The overall velocity profile and flow properties near stretched sheet are modified by the combined effects of buoyancy and suction. Near stretched surface, the flow slows down due to buoyancy forces. There are decreased velocities close to the sheet's surface because of the hotter fluid moving upward and pushing the colder fluid lower.

For various estimates of the porosity parameter P, Fig.5 shows velocity profiles f′(η). The porosity or permeability of a porous substance is commonly indicated by the porous factor. The method for calculating

the volume of fluid passing through a porous media is detailed in the statement. Fluid flow is more restricted when the porosity parameter P is higher since it indicates a smaller permeable medium k. Consequently, this causes the speed to decrease close to the stretched surface.

Figure 6 shows the temperature circulation of thermal boundary layer for various values of the thermophoresis factor Nt. Thermophoresis is a transport mechanism induced by a temperature gradient. The boundary layer becomes heavier as Nt increases, which raises the surface temperature and indicates that the temperature is growing.

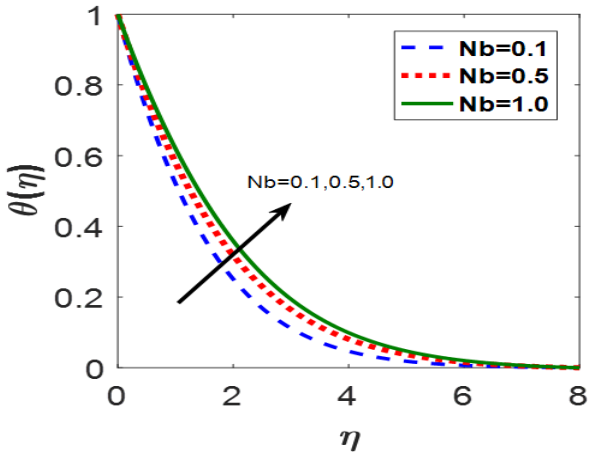


Fig.7. Temperature v/s Brownian motion.

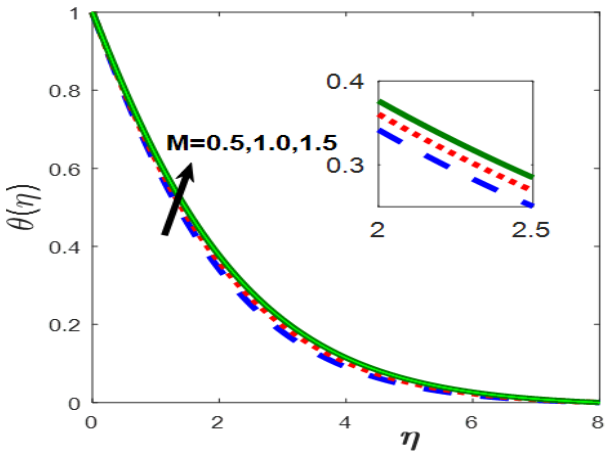


Fig.8. Temperature v/s magnetic parameter.

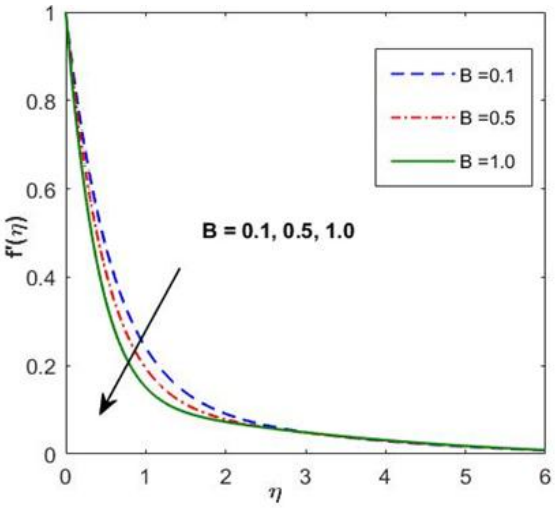


Fig.9. Velocity v/s Maxwell parameter.

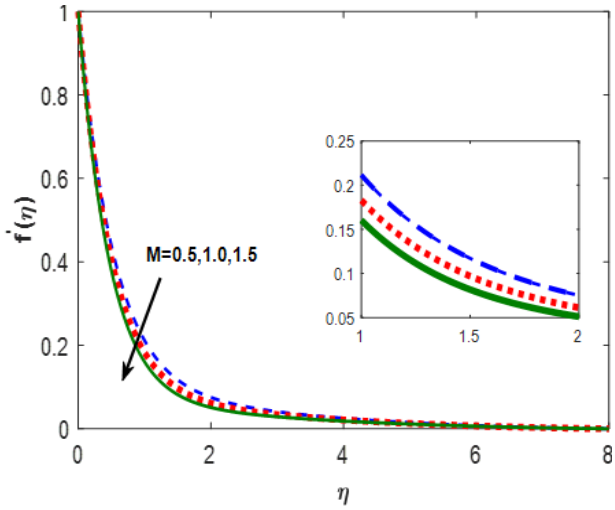


Fig.10. Velocity v/s magnetic parameter.

For multiple Brownian motion Nb computations, Fig.7 displays the thermal BL temperature dispersion. When molecules in a fluid collide with one another often, the resulting motion is known as Brownian motion. This erratic motion exacerbates the collisions between nano particles and fluid molecules. Temperature rises as molecules convert their kinetic energy into thermal energy.

Temperature distributions plotted against the magnetic variable M are shown in Fig.8. As M becomes larger, the temperature rises as well. This is because an increase in the value of M results in a wider temperature spread since it decreases the nanofluid's velocity.

In Fig.9, we can see the effect of the Maxwell parameter B on the distribution of velocities $f'(\eta)$. As B increases, $f'(\eta)$ drops in this case. The amount of time it takes for a liquid to go back to its original state after a force has been applied is called the relaxation time (B). In a fluid, a greater B value suggests solid-like properties, whereas a lower B value suggests liquid-like ones. Higher B values cause the viscosity of the fluid to rise, which in turn causes the flow resistance to rise and the velocity to fall.

Figure 10 shows how M effects the velocity profile and shows that a small change in M results in a reduction. The magnetic component reduces the velocity distribution by producing a resistive force that prevents the fluid from flowing.

Lewis number provides a numerical value for the ratio of mass transfer to heat transfer. Among magnetohydrodynamic (MHD) nanofluids, the concentration profiles are significantly influenced by the Lewis number. Impact of Lewis number on concentration profiles is depicted in Fig.11. It is evident from the plots that the temperature A higher Lewis number causes the species to condense into smaller areas, which in turn causes the gradients to be more pronounced and the bulk concentrations of the fluid to be lower. The main reason for the decrease in concentration is because heat diffusivity has a more significant impact in limiting the spreading of the species in the fluid than mass diffusivity.

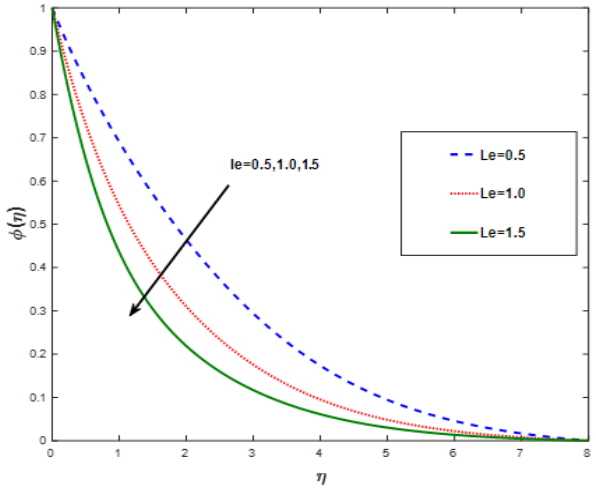


Fig.11. Concentration v/s Lewis number.

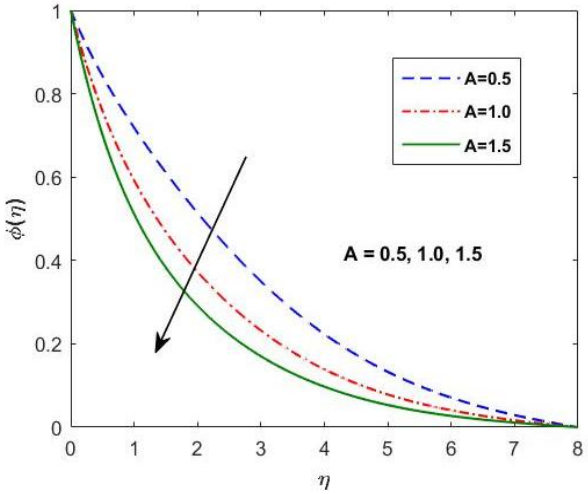


Fig.12. Concentration v/s chemical reaction.

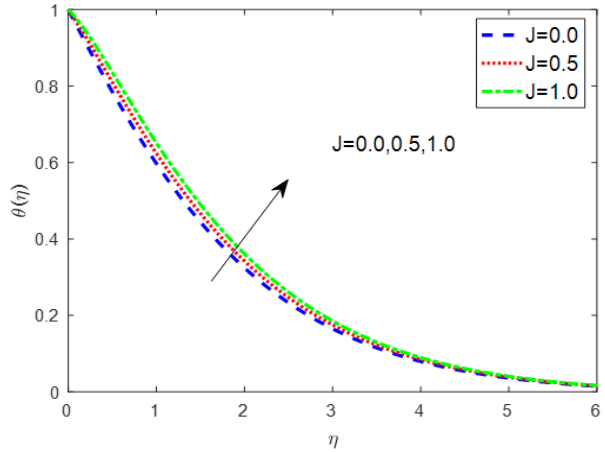


Fig.13. Temperature v/s Joule heating parameter.

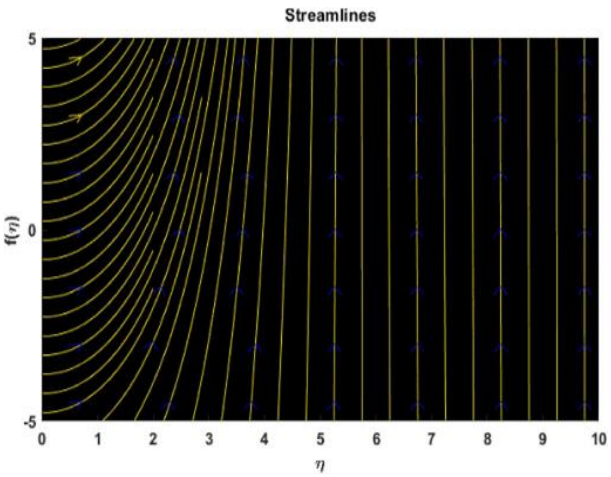


Fig.14. flow field streamlines.

The contribution of A to the concentration decline is examined in Fig.12, which shows a more intense chemical reaction. Scaling A predictions reduce the buoyancy influence on concentration, which results in a decrease in concentration.

Joule heating occurs in MHD nanofluid systems due to the passage of current via the conductive fluid. The rise in temperature is induced by the Joule heating phenomenon in an MHD nanofluid which is clearly displayed in Fig.13. This is because, for a given amount of current, the increase in heat generation is directly proportional to the nanoparticles' enhancement of electrical conductivity. The fluid's temperature rises due to the heat created by Joule heating.

The differential equations regulate the flow according to the designated boundary conditions, and the streamlines shown in Fig.14 represent this flow pattern. Areas with closely spaced streamlines signify elevated velocities, whilst areas with widely spaced streamlines denote reduced velocities; the streamlines visually represent the direction and relative speed of fluid particles within the flow domain.

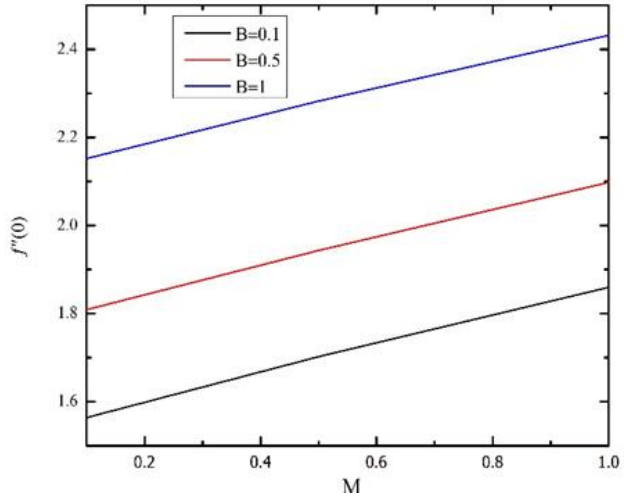


Fig.15. Magnetic Parameter v/s $f''(0)$.

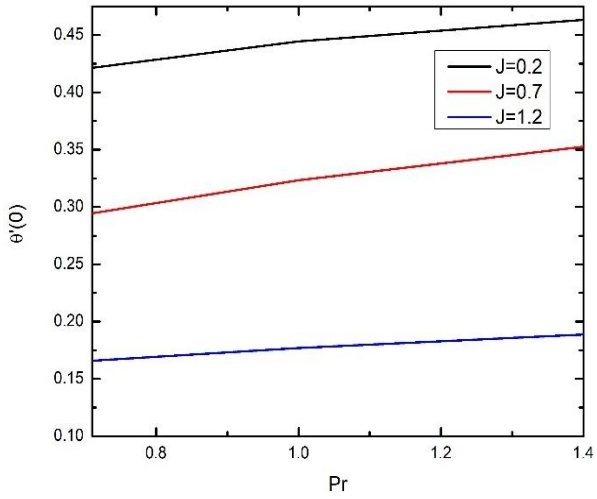


Fig.16. Prandtl number v/s $\theta'(0)$.

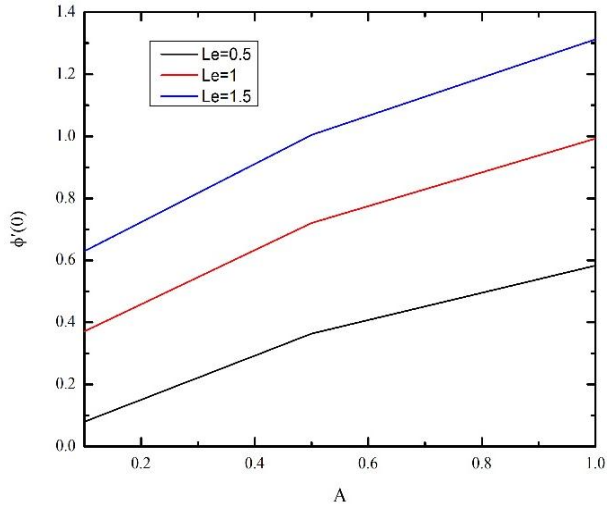


Fig.17. Chemical reaction v/s $\phi'(0)$.

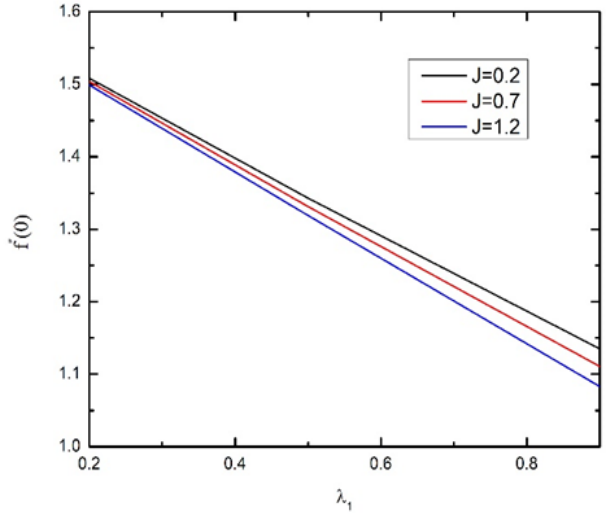


Fig.18. Thermal buoyancy factor v/s $f''(0)$.

Figure 15 illustrates that skin friction values escalate with the increasing values of the magnetic field parameter and the Maxwell parameter. Figure 16 illustrates that the Nusselt number diminishes as the values

of Prandtl number and J increase. Figure 17 reveals that elevated values of chemical reaction and Lewis number correspond to an increase in mass transfer rate.

The direction of the interaction between buoyant force and incoming flow determines whether thermal buoyancy has a positive or negative effect on flow and heat transfer. The upward buoyant force that a fluid with a higher concentration of solute experiences when surrounding by a fluid with a lower concentration of the same solute is known as concentration buoyancy. Figure 18 shows the relationship of skin friction with the thermal buoyancy parameter of different opposing flow parameter values J.

Table 1 reveals the intriguing information on Skin friction, Nusselt, and Sherwood numbers for different parameters. Numerical values of rate of skin friction, heat, and mass transfer coefficient for variation of M, Nb, λ_1, λ_2, B, Le, Pr, Nt, J, A, P, S, $f''(0)$, $\theta'(0)$ and $\phi'(0)$ is displayed in Tab.1. It is evident from the tabulated values that with the increasing values of thermal buoyancy and concentration parameters, Skin friction coefficient is reduced whereas the Nusselt, and Sherwood numbers are increasing. Also, skin friction, Nusselt, and Sherwood numbers are decreasing with the increasing values of Joule heating parameter.

Table 1. Skin friction, Nusselt, and Sherwood numbers for different parameters.

M	Nb	λ_1	λ_2	B	Le	Pr	Nt	J	A	P	S	$-f''(0)$	$-\theta'(0)$	$-\varphi'(0)$
0.1												*1.563538*	*0.401424*	*0.079634*
0.5												*1.701920*	*0.390617*	*0.083393*
1												*1.859248*	*0.378913*	*0.088157*
	0.5											*1.56358*	*0.401424*	*0.079634*
	1											*1.570013*	*0.335089*	*0.265868*
	1.5											*1.570777*	*0.277596*	*0.325571*
		0.1										*1.563538*	*0.401424*	*0.079634*
		0.5										*1.342949*	*0.424453*	*0.074749*
		0.9										*1.134886*	*0.440305*	*0.071907*
			0.1									*1.563538*	*0.401424*	*0.079634*
			0.4									*1.341943*	*0.432817*	*0.080144*
			0.9									*0.996841*	*0.459764*	*0.084432*
				0.1								*1.563538*	*0.401424*	*0.079634*
				0.5								*1.808928*	*0.385066*	*0.087329*
				1								*2.152023*	*0.367161*	*0.097285*
					0.5							*1.563538*	*0.401424*	*0.079634*
					1							*1.576449*	*0.369019*	*0.371053*
					1.5							*1.585076*	*0.350785*	*0.620994*
						0.71						*1.563538*	*0.401424*	*0.079634*
						1						*1.570821*	*0.474540*	*0.107387*
						1.4						*1.579419*	*0.535205*	*0.180893*
							0.5					*1.563538*	*0.401424*	*0.079634*
							0.6					*1.560360*	*0.394336*	*0.025761*
							1.5					*1.535762*	*0.333951*	*0.351123*
								0.2				*1.563538*	*0.401424*	*0.079634*
								0.7				*1.561284*	*0.294647*	*0.069971*
								1.2				*1.558988*	*0.185792*	*0.061435*
									0.1			*1.563538*	*0.401424*	*0.079634*
									0.5			*1.574898*	*0.373661*	*0.363231*
							0.6					*1.560360*	*0.394336*	*0.025761*

Table 1.cont. Skin friction, Nusselt, and Sherwood numbers for different parameters.

M	Nb	λ_1	λ_2	B	Le	Pr	Nt	J	A	P	S	$-f''(0)$	$-\theta'(0)$	$-\varphi'(0)$
							1.5					*1.535762*	*0.333951*	*0.351123*
								0.2				*1.563538*	*0.401424*	*0.079634*
								0.7				*1.561284*	*0.294647*	*0.069971*
								1.2				*1.558988*	*0.185792*	*0.061435*
									0.1			*1.563538*	*0.401424*	*0.079634*
									0.5			*1.574898*	*0.373661*	*0.363231*
									1			*1.582452*	*0.357028*	*0.582630.*
										0.1		*1.563538*	*0.401424*	*0.079634*
										0.5		*1.701920*	*0.390617*	*0.083393.*
										1		*1.859248*	*0.378913*	*0.088157*
											0.3	*1.563538*	*0.401424*	*0.079634*
											0.5	*1.713788*	*0.491726*	*0.030480*
											0.6	*1.797981*	*0.538550*	*0.004672*

Table 2 compares estimates for the Nusselt number, along with approximations for Nb and $S = 1.5$ in the absence of A and M .

Table 2. Comparison of Nusselt number estimates and approximations for Nb and $S = 1.5$ in the absence of A and M .

Nb	Published result [24] of $-\theta'(0)$	Present Nusselt number values $-\theta'(0)$
0.2	*1.142490*	*1.142670*
0.8	*0.942560*	*0.941850*
1.2	*0.831832*	*0.831743*
1.7	*0.750881*	*0.750189*

5. Conclusion

The goal of this research is to determine how Maxwell nanofluid moves over a porous vertical stretching surface in response to Joule heating effects and magnetic field chemical reactions. By applying the right similarity transformations, nonlinear PDEs may be transformed into nonlinear ODEs. This article uses a shooting approach that makes use of the R-K strategy to generate numerical results.

The present results are summarized here:

- A perceived slowing of speed may occur when the magnetic component increases. a magnetic element that, when combined with the fluid, produces a resistance, and so stops its flow.
- Concentration profiles generally diminish as the intensity of the chemical reaction increases. Enhanced estimations of the chemical reaction constant A diminish the impact of buoyancy on concentration, leading to reduced concentration levels.
- Temperature profiles vary with an increase in the Brownian motion parameter. Brownian motion refers to the erratic movement of particles within fluids, resulting from continuous molecular collisions. Volatile motion enhances the frequency of fluid nanoparticle collisions. Temperature rises as molecules transform kinetic energy into thermal energy.
- The phenomenon of Joule heating is to raise the temperature of the fluid.

Acknowledgments

The authors thank the reviewers and editor for their helpful comments, which made this work better. The authors thank the people in charge of MG University and SNIST for giving them the tools they needed to do the research.

Nomenclature

A – chemical reaction parameter
B – Maxwell parameter
BL – boundary layer
c_p – the specific heat at constant pressure $\left[\frac{Kg}{ms^2}\right]$
D_B – mass diffusion
J – Joule heating parameter
k – permeability
Le – Lewis number
M – magnetic parameter
MHD – magnetohydrodynamics
MNF – Maxwell Nanofluid
Nb – Brownian motion
Nt – thermophoresis
$ODEs$ – ordinary differential equations
P – porosity factor
$PDEs$ – partial differential equations
Pr – Prandtl number
q_m – mass flux
q_w – radiative heat flux $\left[\frac{W}{m^2}\right]$
S – suction parameter
Sc – Schmidt number
u,v – velocity components $\left[\frac{m}{s}\right]$
x,y – axis coordinates $[m]$
α – thermal diffusivity $\left[\frac{m^2}{s}\right]$
λ_1 – Thermal buoyancy factor
λ_2 – Concentration buoyancy factor
ν – kinematic viscosity $\left[\frac{m^2}{s}\right]$
ρ – fluid's density $\left[\frac{Kg}{m^3}\right]$
τ_w – drag factor

References

[1] Mukhtar T., Jamshed W., Aziz A. and Al-Kouz W. (2023): *Computational investigation of heat transfer in a flow subjected to magnetohydrodynamic of Maxwell nanofluid over a stretched flat sheet with thermal radiation*.– Numer. Methods Part. Differ. Equ., vol.39, No.5, pp.3499-3519, https://doi.org/10.1002/num.22643.

[2] Srilatha P., Abu-Zinadah H., Kumar R.S.V., Alsulami M.D., Kumar R.N., Abdulrahman A. and Punith Gowda R.J. (2023): *Effect of nanoparticle diameter in Maxwell nanofluid flow with thermophoretic particle deposition*.– Mathematics, vol.11, No.16, pp.3501, https://doi.org/10.3390/math11163501.

[3] Kumar M.A. and Reddy Y.D. (2023): *Thermal radiation and chemical reaction influence on MHD boundary layer flow of a Maxwell fluid over a stretching sheet containing nanoparticles*.– J. Therm. Anal. Calorim., vol.148, No.13, pp.6301-6309, https://doi.org/10.1007/s10973-023-12097-1.

[4] Ahmad S., Khan M.N., Nadeem S., Rehman A., Ahmad H. and Ali R. (2021): *Impact of Joule heating and multiple slips on a Maxwell nanofluid flow past a slendering surface*.– Commun. Theor. Phys., vol.74, No.1, pp.015001, https://doi.org/10.1088/1572-9494/ac3bc8.

[5] Irfan M., Khan M. and Khan W.A. (2020): *Heat sink/source and chemical reaction in stagnation point flow of Maxwell nanofluid*.– Appl. Phys. A, vol.126, pp.1-8, https://doi.org/10.1007/s00339-020-04051-x.

[6] Sadiq M.A., Waqas M., Hayat T. and Alsaedi A. (2019): *Modeling and analysis of Maxwell nanofluid considering mixed convection and Darcy-Forchheimer relation*.– Appl. Nanosci., vol.9, pp.1155-1162, https://doi.org/10.1007/s13204-019-00968-9.

[7] Upreti H., Bisht A. and Joshi N. (2024): *MHD Darcy-Forchheimer flow and double-diffusive modeling of Maxwell fluid over rotating stretchable surface: a computational study*.– Mod. Phys. Lett. B, pp.2450227, https://doi.org/10.1142/S0217984924502270.

[8] Zhang L., Vaddemani R.R., Ganjikunta A., Bingi S. and Kodi R. (2024): *3D-MHD mixed convection in a Darcy-Forchheimer Maxwell fluid: thermo diffusion, diffusionthermo effects, and activation energy influence*.– Case Stud. Therm. Eng., pp.104916, https://doi.org/10.1016/j.csite.2024.104916.

[9] Ahmadian A., Bilal M., Khan M.A. and Asjad M.I. (2020): *The non-Newtonian Maxwell nanofluid flow between two parallel rotating disks under the effects of magnetic field*.– Sci. Rep., vol.10, No.1, pp.17088,,https://doi.org/10.1038/s41598-020-74096-8.

[10] Ijaz M. and Ayub M. (2019): *Nonlinear convective stratified flow of Maxwell nanofluid with activation energy*.– Heliyon, vol.5, No.1, pp.e01121, https://doi.org/10.1016/j.heliyon.2019.e01121.

[11] Khan M., Irfan M. and Khan W.A. (2019): *Heat transfer enhancement for Maxwell nanofluid flow subject to convective heat transport*.– Pramana, vol.92, No.2, pp.17, https://doi.org/10.1007/s12043-018-1690-2.

[12] Irfan M., Khan M., Khan W.A. and Ayaz M. (2018): *Modern development on the features of magnetic field and heat sink/source in Maxwell nanofluid subject to convective heat transport*.– Phys. Lett., vol.382, No.30, pp.1992-2002, https://doi.org/10.1016/j.physleta.2018.05.008.

[13] Ramzan M., Bilal M., Chung J.D. and Farooq U. (2016): *Mixed convective flow of Maxwell nanofluid past a porous vertical stretched surface-an optimal solution*.– Results Phys., vol.6, pp.1072-1079, https://doi.org/10.1016/j.rinp.2016.11.036.

[14] Venkatesh N., Raju R.S., Kumar M.A. and Reddy Y.D. (2024): *A numerical study on MHD Maxwell fluid with nanoparticles over a stretching surface: impacts of thermal radiation, convective boundary condition and induced magnetic field*.– Numer. Heat Tran. Part A: Applications, pp.1-16, https://doi.org/10.1080/10407782.2024.2338259.

[15] Shi S., Niu J., Wu Z., Luo S., Gao X., Fang Y. and Zhang Z. (2022): *Experimental and numerical investigation on heat transfer enhancement of vertical triplex tube heat exchanger with fractal fins for latent thermal energy storage*.– International Journal of Heat and Mass Transfer, https://doi.org/10.1016/j.ijheatmasstransfer.2022.123386.

[16] Rasheed A.H., Alias H.B. and Salman S.D. (2021): *Experimental and numerical investigations of heat transfer enhancement in shell and helically microtube heat exchanger using nanofluids*.– International Journal of Thermal Sciences, https://doi.org/10.1016/j.ijthermalsci.2020.106547.

[17] Wang Y.B., Huang L.F., Lan N., Wang S.L., Zhang B.X., Yang Y.R., Wang X.D. and Lee D.J. (2024): *Heat transfer enhancement by electro hydrodynamics in wavy channels*.– Applied Thermal Engineering, https://doi.org/10.1016/j.applthermaleng.2023.121556.

[18] Fico F., Langella I. and Xia H. (2023): *Large-eddy simulation of magnetohydrodynamics and heat transfer in annular pipe liquid metal flow*.– Physics of Fluids, https://doi.org/10.1063/5.0143687.

[19] Yang X., Yu J., Guo Z., Jin L. and He Y.L. (2019): *Role of porous metal foam on the heat transfer enhancement for a thermal energy storage tube*.– Applied Energy, https://doi.org/10.1016/j.apenergy.2019.01.075.

[20] Mousa M.H., Miljkovic N. and Nawaz K. (2021): *Review of heat transfer enhancement techniques for single phase flows*.– Renewable and Sustainable Energy Reviews, https://doi.org/10.1016/j.rser.2020.110566.

[21] Dulikravich G.S. and Lynn S.R. (1997): *Unified electro-magneto-fluid dynamics (EMFD): a survey of mathematical models*.– International Journal of Non-Linear Mechanics, vol.32, No.5, pp.923-932, https://doi.org/10.1016/S0020-7462(96)00083-2.

[22] Davidson P.A. (2016): *Introduction to Magnetohydrodynamics*.– Cambridge University Press. https://doi.org/10.1017/9781316672853.

[23] Sheikholeslami M. and Rokni H.B. (2017): *Simulation of nanofluid heat transfer in presence of magnetic field: a review*.– Int. J. of Heat and Mass Transfer, vol.115, pp.1203-1233, https://doi.org/10.1016/j.ijheatmasstransfer.2017.08.108.

[24] Reddy M.S. and Kumar M.A. (2024): *Influence of magnetic field chemical reaction and Soret-Dufour parameters on Maxwell nanofluid flow over a porous vertical stretching surface-a numerical study*.– Case Studies in Chemical and Environmental Engineering. pp.100958, https://doi.org/10.1016/j.cscee.2024.100958.

[25] Xu H.J., Xing Z.B., Wang F.Q. and Cheng Z.M. (2019): *Review on heat conduction, heat convection, thermal radiation, and phase change heat transfer of nanofluids in porous media: fundamentals and applications*.– Chemical Engineering Sciences, vol.195, pp.462-483, https://doi.org/10.1016/j.ces.2018.09.045.

[26] Ghaderi E., Bijarchi M.D.A., Hannani S.K. and Boroujerdi N. (2024): *Evaluating Joule heating's influence on heat transfer and entropy generation in MHD channel flow: a parametric study and ill-posed problem solution using PINNs*.– https://doi.org/10.13140/RG.2.2.35691.35365.

[27] Yuvaraju N., Hymavathi D., Ramesh K. and Reddy B.S. (2024): *Joint effect of velocity slip and Joule heating MHD Casson-Williamson nanofluid passes through the stretching porous medium*.– Journal of Advanced Research in Fluid Mechanics and Thermal Sciences vol.123, No.1, pp.156-171. https://doi.org/10.37934/arfmts.123.1.156171.

[28] Ramesh K., Naik H.S., Reddy B.S. and Christophe C. (2022): *Role of nanoparticles and heat source/sink on MHD flow of Cu-H2O nanofluid flow past a verticle plate with Soret and Dufour effects*.– Mathematical and Computational Applications, vol.27, No.102, pp.1-18, https://doi.org/10.3390/mca27060102.

[29] Reddy B.N., Maddileti P. and Reddy B.S. (2022): *Nanofluid flow on non-linearly stretching surface influenced by the combined effects of Soret and Dufour with chemical reaction*.– JP Journal of Heat and Mass Transfer, vol.30, pp.161-182, https://doi.org/10.17654/0973576322062.

[30] Ravikiran C., Halesh K., Reddy B.S. and Saritha K. (2024): *Mechanisms of diffusion thermo and thermal diffusion on MHD mixed convection flow of Casson fluid over a vertical cone with porous material in the presence of thermophoresis and a Brownian motion*.– Journal of Advanced Research in Numerical Heat Transfer, vol.7, No.1, pp.29-43, https://doi.org/10.37934/arnht.17.1.2943.

[31] Sheikhzdeh G.A., Qomi M.E., Hajialigol N. and Fattahi A. (2012): *Numerical study of convection flows in a lid-driven enclosure filled with nanofluid using variable properties*.– Results in Physics, vol.2, pp.5-13, https://doi.org/10.1016/j.rinp.2012.01.001.

[32] Malga B.S., Srisailam B., Reddy K.S. and Narender G. (2023): *The effect of viscous dissipation and chemical reaction on the flow of MHD nanofluid*.– Journal of Advanced Research in Fluid Mechanics and Thermal Sciences, vol.107, No.2, pp.150-170, https://doi.org/10.37934/arfmts.107.2.150170.

[33] Mangamma C., Malga B.S., Kumar P.P. and Appidi L. (2024): *Magnetohydrodynamic boundary layer flows over a moving porous vertical plate with viscous dissipation and Dufour effects in the presence of heat source and chemical reaction*.– Journal of Advanced Research in Numerical Heat Transfer, vol.26, No.1, pp.99-113, https://doi.org/10.37934/arnht.26.1.99113.

[34] Turkyilmazoglu M. (2026): *A unified Stefan-Scott theory for squeeze-film lubrication between non-uniformly deforming boundaries*.– International Communications in Heat and Mass Transfer, vol.174, pp.111012, https://doi.org/10.1016/j.icheatmasstransfer.2026.111012.

[35] Turkyilmazoglu M. and Pop I. (2023): *Induced flow and heat transfer due to inner stretching and outer stationary coaxial cylinders*.– International Communications in Heat and Mass Transfer, vol.146, pp.106903, https://doi.org/10.1016/j.icheatmasstransfer.2023.106903.

Received: April 22, 2026
Revised: July 20, 2026